Carcinogenesis, 2018, Vol. 39, No. 2, 109–117

doi:10.1093/carcin/bgx116
Advance Access publication October 24, 2017
Original Article

ORIGINAL ARTICLE

Cellular shear stiffness reflects progression of arsenic-induced transformation during G_1

Alexandra Muñoz[1,2,†], Will J. Eldridge[3,†], Nina Munkholt Jakobsen[4,5], Helle Sørensen[4], Adam Wax[3] and Max Costa[1,*]

[1]Department of Environmental Medicine, New York University School of Medicine, Tuxedo, NY 10987, USA, [2]Centre for Symmetry and Deformation, Department of Mathematical Sciences, University of Copenhagen, 2100 Copenhagen Ø, Denmark, [3]Department of Biomedical Engineering, Duke University, Durham, NC 27708, USA, [4]Laboratory for Applied Statistics, Department of Mathematical Sciences, University of Copenhagen, 2100 Copenhagen Ø, Denmark and [5]Department of Applied Mathematics and Computer Science, Technical University of Denmark, 2800 Kgs. Lyngby, Denmark

*To whom correspondence should be addressed. Tel: +1 (845)-731-3515; Fax: +1 (845)-351-2118; Email: max.costa@nyumc.org
Correspondence should also be addressed to Adam Wax. Tel: +1 (919) 660-5143; Fax: +1 (919) 684-4488, Email: a.wax@duke.edu
Correspondence should also be addressed to Alexandra Muñoz. Tel: (+45) 35 32 07 23; Fax: (+45) 35 32 95 55, Email: alexandra@math.ku.dk

†These authors contributed equally to this work.

Abstract

Cancer cells consistently exhibit decreased stiffness; however, the onset and progression of this change have not been characterized. To study the development of cell stiffness changes, we evaluated the shear stiffness of populations of cells during transformation to a carcinogenic state. Bronchial epithelial cells were exposed to sodium arsenite to initiate early stages of transformation. Exposed cells were cultured in soft agar to further transformation and select for clonal populations exhibiting anchorage-independent growth. Shear stiffness of various cell populations in G1 was assessed using a novel non-invasive assay that applies shear stress with fluid flow and evaluates nanoscale deformation using quantitative phase imaging (QPI). Arsenic-treated cells exhibited reduced stiffness relative to control cells, while arsenic clonal lines, selected by growth in soft agar, were found to have reduced stiffness relative to control clonal lines, which were cultured in soft agar but did not receive arsenic treatment. The relative standard deviation (RSD) of the stiffness of Arsenic clones was reduced compared with control clones, as well as to the arsenic-exposed cell population. Cell stiffness at the population level exhibits potential to be a novel and sensitive framework for identifying the development of cancerous cells.

Introduction

Cancers exhibit widespread genetic diversity while simultaneously forming consistent biomechanical structures, tumors, which foster the development of diverse cell populations essential to tumor growth and metastasis. From a biomechanical perspective, tumor development requires tightly regulated mechanical properties including the formation of a stiff extracellular matrix (ECM) and deformable metastatic cell phenotypes (1). Such mechanical properties are increasingly recognized as robust indicators of cancer progression, where cellular deformability and tumor stiffness can be used to determine malignancy and assess metastatic potential (1–5). Numerous studies indicate that cancer cells from diverse developmental processes and tissue origins exhibit reduced cellular stiffness relative to non-cancer cells (2,3,6–8). Here, we explore the onset of cellular stiffness changes during various stages of arsenic-induced cellular transformation to evaluate whether subtle changes in cellular stiffness are detectable and to preliminarily assess whether such changes have potential as a biomarker of cell transformation.

To understand the relevance and complexity of cellular stiffness as a biomarker of transformation, it is necessary to emphasize the role of extracellular remodeling in cancer progression

Received: May 12, 2017; **Revised:** October 9, 2017; **Accepted:** October 19, 2017

Abbreviations

COM	center-of-mass
ECM	extracellular matrix
LR	likelihood ratio
ML	maximum likelihood
RSD	relative standard deviation
REML	restricted ML
QPI	quantitative phase imaging
OPL	optical path length

and development of tumor subpopulations. During carcinogenesis, extracellular deposition of collagen and vascularization remodel the ECM, generating physical niches with distinct biomechanics (shear force upon cells, crowding) and chemical features (hypoxia, drivers of growth signaling). This spatial heterogeneity promotes the development of subpopulations, including metastatic populations, within the tumor through local selective pressures leading to the distribution of key cancer features across cooperating subpopulations (9–11). Additionally, ECM stiffening can promote a cellular process known as epithelial to mesynchymal transition, during which cells lose features of differentiated epithelial cells and gain features of more motile mesynchymal cells, such as anchorage-independent growth (12,13). These cells are hypothesized to migrate out of the tumor via 'collagen highways', potentially making epithelial to mesynchymal transition and cell deformability key aspects of metastasis (12–14). Therefore, development of a stiffness biomarker presents an opportunity to view the process of carcinogenesis through a single property that may simultaneously reflect ECM remodeling and development of metastatic phenotypes. Given the interplay of ECM remodeling and tumor subpopulations, we focus upon cellular stiffness of a population of cells, rather than individual cells, when evaluating its potential as a biomarker.

The goal of our study is to assess whether cell stiffness can reflect the progression of cell transformation. We capture cells at early and late stages of transformation to assess whether subtle changes in cellular stiffness can be detected and whether early and late stages are distinguishable. To our knowledge, no studies have been conducted to evaluate cellular stiffness changes during transformation nor in early stages of carcinogenesis. Thus, the cell culture procedure in this study is intended to serve as a proxy for *in situ* carcinogenesis and is used here to preliminarily gauge the utility of stiffness as a biomarker during early stages of transformation.

To begin the transformation process, cells were exposed to inorganic arsenic, a carcinogen with a broad mechanistic impact that is known to promote a range of different types of cancer including bladder, lung and prostate cancers (15–19). Arsenic exerts its intracellular influence through a wide range of molecular interactions (17–20) that make it ideally suited to promote a proxy transformation process that is reflective of a true *in situ* process. After 4 weeks of arsenic exposure, we then selected for cells exhibiting anchorage-independent growth by seeding cells in soft agar. Anchorage-independent growth is important during metastasis and is a key identifying feature of cancer cells and transformed cells (21,22). The shift in extracellular tension mediated by the agarose also advances the transformation process (4). Following development of these cell lines, we employed a novel method that utilizes fluid flow to apply shear stress and quantitative phase imaging (QPI) to assess nanoscale levels of cellular deformation in response to the applied pressure (23). Unlike other methods that involve exogenous contact or application of dye, our method allows cells to maintain normal attachment and media conditions during measurement. Furthermore, this method allows for measurement of large sample sizes permitting detection of subtle differences in stiffness at the population level. The sensitivity of this method in combination with the known phylogeny of cell populations permits analysis of stiffness changes during development rather than solely assessing it at the end point of the process.

Materials and methods

Cell culture protocol

Immortalized human bronchial epithelial cells (BEAS-2B#CRL-9609, ATCC, Manassas, VA) were cultured in Dulbecco's Modified Eagle Medium (#11995-065, Life Technologies) supplemented with 10% fetal bovine serum (Atlanta Biologicals) and 1% Penstrep (#15140-122, Life Technologies). Cells were maintained at 37°C with 5% CO_2 and 100% humidity. All cells were a gift from Haobin Chen at New York University School of Medicine. Cells were cultured from mid-March 2015 to July 2015 for this experiment and were passaged every 4 days with media changes every 2 days using 0.05% trypsin (GIBCO). Human lung carcinoma cells (A549 #CRM-CRL-185, ATCC, Manassas, VA) were cultured in F-12K media (#21127022, Thermo Fischer Scientific) supplemented and cultured as above during July 2015. The BEAS-2B and A549 cell lines were authenticated in July 2015 and October 2017, respectively, by Genetica DNA Laboratories. BEAS-2B and A549 cells were authenticated via short tandem repeat profiling and each exhibited a 100% match to their reference profiles, BEAS-2B (ATCC CRL-9609) and A549 (ATCC CCL-185), respectively.

Cell populations

The phylogenetic relationships and the process for developing the cell populations used in this study are illustrated in Figure 1. All other graphs and figures are color coded to match this figure. The cellular populations are briefly introduced here. 'Arsenic 4w' and 'Arsenic 12w' are BEAS-2B cells exposed to arsenic for 4 and 12 weeks, respectively. 'BEAS-2B' is the control population cultured under the same conditions for 4 weeks but without arsenic exposure. Arsenic 4w cells were then seeded in soft agar and allowed to form colonies for an additional 4 weeks, after which individual colonies were extracted and re-established as monolayer clonal cell lines. Cells from these clonal cell lines were measured individually for stiffness and form the treatment group 'Arsenic clones'. Correspondingly, BEAS-2B control cells went through the same soft agar process to form the control clones, 'BEAS-2B clones'. The Arsenic 4w and BEAS-2B populations are the parental populations for their respective clonal populations, Arsenic clones and BEAS-2B clones.

Arsenic treatment

For the arsenic exposure, BEAS-2B cells were exposed to sodium meta arsenite (1 μM) ($NaAsO_2$; S7400-100G; Sigma-Aldrich). Sodium meta arsenite was dissolved in Ultra Pure water (#10977-015, Life Technologies), filtered for sterilization with a 0.22 μm filter and added to media after every passage and media change. At 4 weeks, aliquots of BEAS-2B control cells and Arsenic 4w were frozen. Frozen cells were thawed and cultured for 10 days prior to measurement. Arsenic treatment was suspended 48 h prior to stiffness measurement for Arsenic 4w and Arsenic 12w.

Soft agar assay to clonal treatment groups

Cells were seeded at a density of 5×10^3 cells in the top layer of agarose media (0.35% agarose) over the bottom layer (0.5% agarose) in each well of a six-well plate, with no arsenic in media or agarose for either treatment group. Agarose plates were maintained in the incubator for an additional 4 weeks with 200 μl of media added to the wells each week. After 4 weeks, colonies were counted, and numerous individual colonies were extracted from the agarose and re-established as separate monolayer cell lines as previously described (24). The treatment group referred to as Arsenic clones is comprised of cells from five arsenic clonal cell lines, and BEAS-2B clones is comprised of cells from four control clonal cell lines. Clonal cell lines were cultured separately for 4 weeks following the soft agar assay to permit observation of the natural range of stiffness values among the different clonal cell lines, which may vary due to fluctuations in the local microenvironment during development in agar. Since tumors are comprised of subpopulations that develop via local microenvironments (11,25–27), the aim was to approximate such variation by maintaining

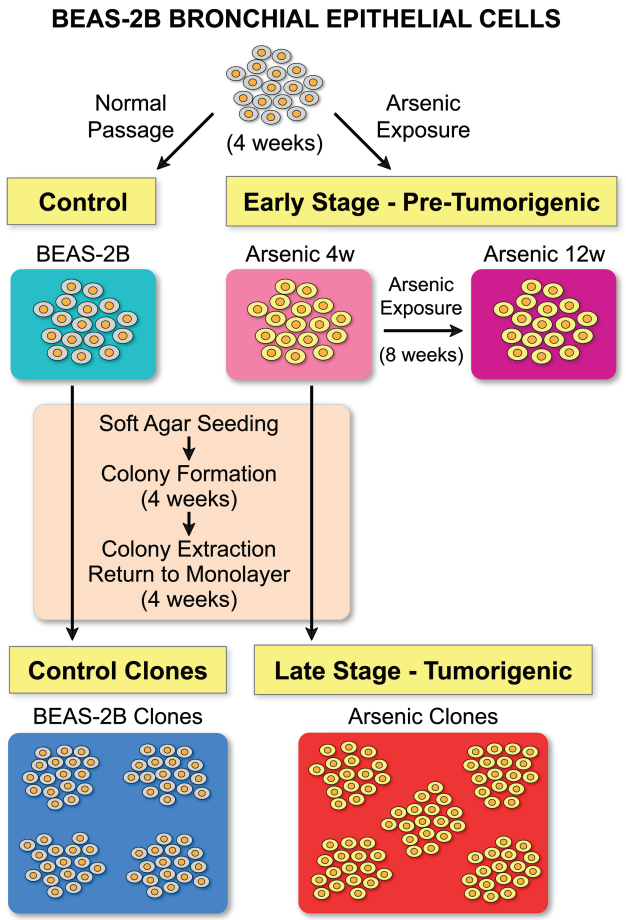

Figure 1. Treatment groups. BEAS-2B human bronchial epithelial cells were cultured for 4 weeks with 1 μM sodium arsenite (Arsenic 4w) and in parallel without arsenic (BEAS-2B). The Arsenic 4w population and the BEAS-2B control population were then seeded in soft agar and allowed to form colonies. At the end of 4 weeks, individual colonies were extracted and re-established as monolayer clonal cell lines. Cells from the five arsenic clonal lines and four BEAS-2B control clonal lines were evaluated to assess cellular stiffness. During analysis, data from the clonal lines was pooled to form the treatment groups Arsenic clones and BEAS-2B clones. Simultaneous to the 8-week process to generate the clonal lines, Arsenic 4w was also continuously exposed to 1 μM sodium arsenite for an additional 8 weeks to form the Arsenic 12w population of cells. The Arsenic 4w and Arsenic 12w comprise the populations representative of early stage carcinogenesis, and the Arsenic clones comprise the population representative of later stage carcinogenesis.

clonal lines separately until the time of stiffness measurement. Stiffness measurements from the five arsenic clonal lines were then pooled to create a proxy for a single tumor. Correspondingly, BEAS-2B clonal lines were also cultured separately and then pooled as the control.

Stiffness measurements

Shear stiffness measurements were obtained through a process that combined high-resolution QPI with fluid induction of shear stress to record cellular displacement in response to the applied force. This novel methodology that combines QPI with a flow cell was previously described in a proof-of-concept study by Eldridge *et al.* (23) and is briefly described below with additional description in Supplementary methods, available at *Carcinogenesis* Online.

Quantitative phase imaging

High-resolution imaging was performed using QPI, in a process that assesses phase delays generated by the object being measured. Phase delays are encoded in the incident light field and detected using interferometric techniques. QPI has previously been implemented to measure mechanical phenomena with nanometer optical path length (OPL) resolution, without the use of contrast agents (23). In QPI, light from a low coherence source is split into a reference beam and a sample beam. The sample beam passes through the object being measured, which imparts a phase delay according to the following relation:

$$\phi(x,y) = 2\pi\Delta n(x,y)d(x,y)/\lambda$$

Here, $\phi(x,y)$ is the phase delay of the incident light field, λ is the wavelength of the incident light wave, $d(x,y)$ is the axial depth of the object and $\Delta n(x,y)$ is the refractive index difference between the sample and the surrounding media (23,28–30). From the phase information, the optical path length (OPL), defined as $OPL(x,y) = \phi(x,y)^*\lambda/2\pi$ at each pixel within the cell, was recorded.

The QPI system used here employs an off-axis holographic technique for phase retrieval (Figure 2) (31). Light from a supercontinuum source (SuperK Compact, NKT Photonics) was spectrally filtered to produce an illumination of center wavelength λ=610 nm, and a bandwidth of $\Delta\lambda$=1 nm, resulting in a coherence length of 214 μm.

Stiffness assessment

The day prior to cell stiffness measurement, cells were split and plated at a density of about 1000–3000 cells in 250 μL of complete media on 40 mm round glass coverslips (Warner Instruments, CS-40R) inside a 60 mm dish to maintain sterility and humidity conditions. For measurement, complete media was gently removed from the glass coverslip using a pipette, and the coverslip was inserted into the closed chamber flow cell (Bioptechs, FCS3) mounted onto the optical setup as previously described (23). Cells were imaged for 2 s at zero shear stress, followed by 8 s of imaging during application of 8 dyne/cm^2 (τ_s) shear stress by a syringe pump. Images captured during shear stress application collectively form a video of the cell (Supplementary Videos 1–2, available at *Carcinogenesis* Online). The media used to apply shear stress was Dulbecco's modified eagle medium + 0.25% fetal bovine serum. All images were acquired at 60 fps and an exposure of 16.7 ms using a fast CMOS camera (Fastcam SA4, Photron).

Approximately 30–50 cells were imaged per sample for a period of 30–40 min. During imaging, cells were monitored for signs of intracellular stress (blebbing or detaching), and sample imaging was discontinued if present. Selection of cells for imaging was optimized for imaging conditions by avoiding cells which were in contact with other cells, which may alter the response to shear stress (Supplementary Figure S1, L, available at *Carcinogenesis* Online). For the BEAS-2B-derived cell populations, selection during imaging was optimized to control for the substantial variability in morphology and surface area exhibited by the cells during the different phases of the cell cycle. Progression through the cell cycle is associated with shifts in cell shape, size and the arrangement of nuclear material (32), and cells in different stages of the cell cycle are correlated with cell cycle dependent stiffness magnitudes (33). Given the fluctuation of stiffness over the cell cycle, we restricted sampling to the G_1 phase to reduce the noise introduced by cell cycle variations. To implement this selection, we synchronized cells with the double thymidine block protocol to determine the morphology of the cells during the stages of the cell cycle (34). Cells in G_1 exhibited visually identifiable teardrop (Supplementary Figure S1, Panel A, available at *Carcinogenesis* Online) and near-teardrop shapes (Supplementary Figure S1, Panels B–C, available at *Carcinogenesis* Online). Because the thymidine synchronization involves substantial stress on the cells, we chose to visually select cells during measurement in order to maintain normal culture conditions in the time leading up to stiffness measurement. Further details of the visual identification protocol are described in the supplement with associated OPL images (Supplementary Figure S1, Panels D–K, available at *Carcinogenesis* Online). Post-measurement checks on the visual selection protocol were implemented on image data prior to analysis to confirm that visual selection matched within treatment group G_1 mean cell surface area (Supplementary Methods, available at *Carcinogenesis* Online).

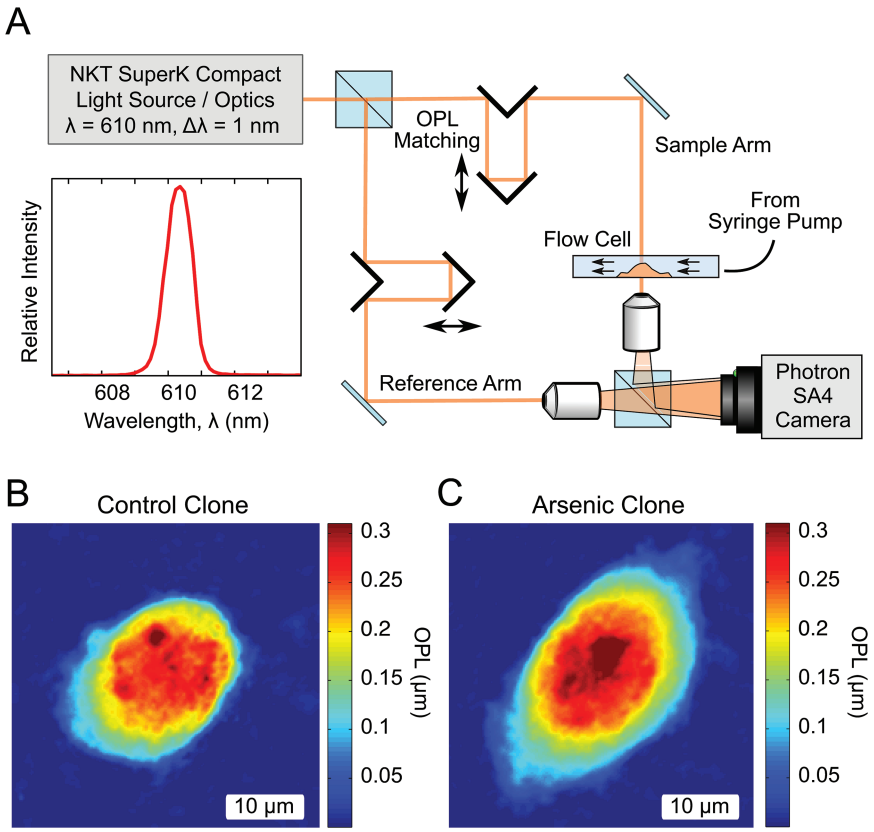

Figure 2. Optical setup and sample images. (**A**) Optical setup. Off-axis quantitative phase system for measuring mechanical displacements due to shear flow. The system employs a Mach-Zehnder holographic configuration by combining the sample light field with a uniform reference field, allowing for calculation of phase delay. The illumination wavelength of 610 nm had a bandwidth of 1 nm, serving to reduce coherence artifacts. OPL matching was implemented to maintain coherence across the field of view. (**B**) and (**C**) Sample OPL maps generated by the setup. OPL images are the product of cell depth and refractive index difference at a given pixel, enabling true quantitative analysis of cellular morphology.

Calculation of effective shear stiffness parameter

The static image of each cell, obtained prior to fluid flow starting, was used as a reference to determine the center-of-mass (COM) of each cell. COM displacement was then determined by tracking COM movement relative to this initial location during the application of shear stress.

The net COM displacement was calculated from the series of images taken during the application of shear flow. The COM position was calculated using custom code (MATLAB R2013a) as previously described and was used to assess COM displacement during shear stress (23). This displacement, $|\vec{r}_{COM}(t)|$, was tracked over time (t) and fit to the following 1D equivalent of the Kelvin–Voigt stiffness model (35):

$$|\vec{r}_{COM}(t)| = \frac{F}{k_s}(1 - e^{-tk_s/\eta})$$

Briefly, the force parameter (F) was obtained as the product of the cell surface area (A_s) and the shear stress of the fluid flow (τ_s). The mechanical application of media from a syringe pump provided a steady shear stress (τ_s) of 8 dyne/cm^2. The geometry of the flow cell ensured uni-directional passage of near laminar flow over the cells (23). Least-square fits were used to fit the COM displacement to the Kelvin–Voigt model in order to obtain the effective shear stiffness parameter (k_s) and the damping parameter (η).

Calculation of cellular orientation during measurement

Static images of each cell were used to obtain orientation during measurement. Major and minor diameters were then calculated by fitting the cell perimeter to an ellipse and recording the axes of the fitted ellipse. From the orientation of these axes, the orientation of the cell with respect to the direction of flow (x-axis of the image) was determined and recorded.

Statistical analysis

Statistical analysis focused on k_s, the shear stiffness in mN/m. Analysis was performed in R (36). Densities were estimated in R using the 'density' function. Stiffness values were transformed by the natural logarithm for analysis, as the non-transformed values exhibited skewed distributions within treatment groups. A linear normal model with log-transformed effective shear stiffness as the response variable was fit to the data from all five treatment groups (the five cellular populations). Treatment and cellular orientation during measurement were included as fixed effects, and within-group standard deviations were allowed to differ for the five treatments. Estimates of the fixed effects in the model along with 95% confidence intervals (CIs) were back-transformed to the original scale of measurement and are presented in Supplementary Table 1, available at *Carcinogenesis* Online. The fixed effects were estimated using maximum likelihood (ML), while the CIs are based on restricted ML (REML) estimates. REML estimates of the within-group standard deviations in the model, here denoted $\hat{\sigma}_g$ for treatment group g, were used to compute model-based estimates of the relative standard deviation (RSD) of effective shear stiffness (on the original scale of measurement) using the formula $\sqrt{\exp(\hat{\sigma}_g^2) - 1}$. Note that an increment in standard deviation on the log scale corresponds to an increment of RSD on the original scale. Plots of orientation by treatment group indicated that observations within each treatment group were evenly spread across the possible values of orientation, meaning that orientation does not distort the interpretation of summary statistics and density plots for the overall populations. However, due to the directionality of the shear flow established in the measurement setup, we opted to correct for cellular orientation in the model.

Each of the pairwise comparisons described in the following was carried out as a separate test within the framework of the model described above. Hypotheses regarding fixed effects were tested using ML likelihood ratio (LR) tests, while tests of hypotheses pertaining to variance parameters were carried out as REML LR tests. The effects of treatment on mean log-transformed effective shear stiffness were compared between the following groups: Arsenic 4w versus BEAS-2B; Arsenic 12w versus BEAS-2B; Arsenic clones versus BEAS-2B clones. On the original scale of measurement, these are interpreted as comparisons of median effective shear stiffness (for a fixed value of orientation). *P*-values from these three tests were Holm–Bonferroni adjusted in order to ensure a family-wise error rate of less than 5%. Furthermore, within-group standard deviations of log-transformed effective shear stiffness were compared between the following treatments: Arsenic 4w versus Arsenic clones; BEAS-2B versus BEAS-2B clones; Arsenic 4w versus BEAS-2B; Arsenic 12w versus BEAS-2B; Arsenic clones versus BEAS-2B clones. These are interpretable as comparisons of within-group RSD of effective shear stiffness on the original scale of measurement. *P*-values from these five tests were Holm–Bonferroni adjusted to ensure a family-wise error rate of less than 5%. Estimation of parameters in the linear normal model, computation of CIs and hypothesis testing were performed using functions from the R package *nlme* (37).

Results

Arsenic-treated cells compared with control BEAS-2B cells

Cells exposed to arsenic were probed for cellular shear stiffness changes to assess whether changes could be detected at the start of cellular transformation. Summary statistics of raw data are presented in Table 1. Figure 3 contains plots illustrating cellular shear stiffness in Arsenic 4w (n = 53), Arsenic 12w (n = 73) and the corresponding control population, BEAS-2B (n = 67). Figure 3A contains box plots of the raw data, while Figures 3B and C contain probability density functions estimated from the raw data and from the log-transformed raw data, respectively, for each treatment group. In these plots, subtle changes are evident in the arsenic-treated populations, which shift left and exhibit less variation relative to the BEAS-2B control population. Estimates from the linear normal model for the treatment effects of the three groups were back-transformed to the original scale and are presented in Figure 3D as estimated median cellular stiffness values (mN/m) for orientation zero, together with corresponding 95% CIs. The LR tests revealed a statistically significant decrease in the median effective shear stiffness of the Arsenic 4w population relative to the BEAS-2B population (P = 0.03) as well as for the Arsenic 12w relative to the BEAS-2B population (P < 0.001). The model-based estimates of RSD were 0.83 for Arsenic 4w, 0.79 for Arsenic 12w and 0.84 for BEAS-2B. There was no significant difference in the RSD of effective shear stiffness for Arsenic 4w relative to BEAS-2B (P = 1), nor for the Arsenic 12w relative to the BEAS-2B population (P = 1).

Arsenic clones compared with BEAS-2B clones

The Arsenic 4w population and BEAS-2B population were seeded in agar and allowed to form colonies for 4 weeks, after which individual colonies were extracted and re-established as monolayer cultures. Size of colonies was variable for both treatment groups. Colony counts from the soft agar assay are presented in Figure 4A. Control cells formed 3, 3 and 2 colonies per well, and the Arsenic 4w population formed 36, 52 and 35 per well. This factor 15 increase in the number of colonies formed in Arsenic 4w over the background level indicates that the cells are transformed, since high levels of anchorage-independent growth is a well-established marker of transformation (21,22,38). Summary statistics of cell stiffness in the treatment groups are presented in Table 1. Figure 4B contains boxplots of the raw data for cells from the individual Arsenic and BEAS-2B clonal lines. There are 1–3 replicate samples from each cell line, and 14–35 cells in each sample, averaging 28 cells per sample. Figure 4C illustrates the pooled data, depicting one box for the Arsenic clones (n = 286) and one for the BEAS-2B clones (n = 224). Figures 4D and E show probability density functions estimated from the raw data and from the log-transformed raw data, respectively, for the two populations. The Arsenic clones clearly exhibit a higher density of lowered stiffness values relative to the BEAS-2B clones. Estimates of treatment effects from the linear normal model, back-transformed to the original scale, are presented in Figure 4F as estimated median cellular stiffness values (mN/m) for orientation zero, together with corresponding 95% CIs. The model-based estimate of RSD for the Arsenic clones was 0.55 and for the BEAS-2B clones was 0.71. The LR tests showed a statistically significant decrease in median effective shear stiffness for Arsenic clones relative to BEAS-2B clones (P < 0.001) as well as a significant decrease in the RSD of the effective stiffness of Arsenic clones relative to the BEAS-2B clones (P = 0.003).

Comparing cell populations before and after agar

To understand the impact of soft agar passage on the arsenic-treated cells and the control cells, we statistically evaluated the difference in RSD of shear stiffness for a given population before (parental) and after agar (clonal). The Arsenic clones that passed through agar had a significantly reduced RSD compared with the Arsenic 4w parental population (P = 0.003), while BEAS-2B clones compared with the BEAS-2B parental population did not have a significantly reduced RSD (P = 0.54). All model-based RSD values are additionally listed in Supplementary Table 2, available at *Carcinogenesis* Online. To further illustrate the impact of agar, Figures 5A and B present the estimated probability density functions of the parental populations with their derived clonal populations based on the log-transformed data. For the Arsenic clones, the probability distribution after agar has reduced mean and standard deviation, reflecting the significant change in the population's stiffness RSD.

Table I. Summary statistics for effective shear stiffness (mN/m)

	Min (mN/m)	Max (mN/m)	Mean (mN/m)	Median (mN/m)	SD	RSD	*n*
Arsenic exposure							
Arsenic 4w	0.24	11.93	2.85	2.32	2.08	0.73	53
Arsenic 12w	0.31	8.64	2.39	1.96	1.71	0.71	73
BEAS-2B	0.60	15.20	4.09	2.65	3.38	0.83	67
Clones							
Arsenic clones	0.33	8.48	2.09	1.91	1.15	0.55	286
BEAS-2B clones	0.51	15.47	3.18	2.50	2.31	0.72	224

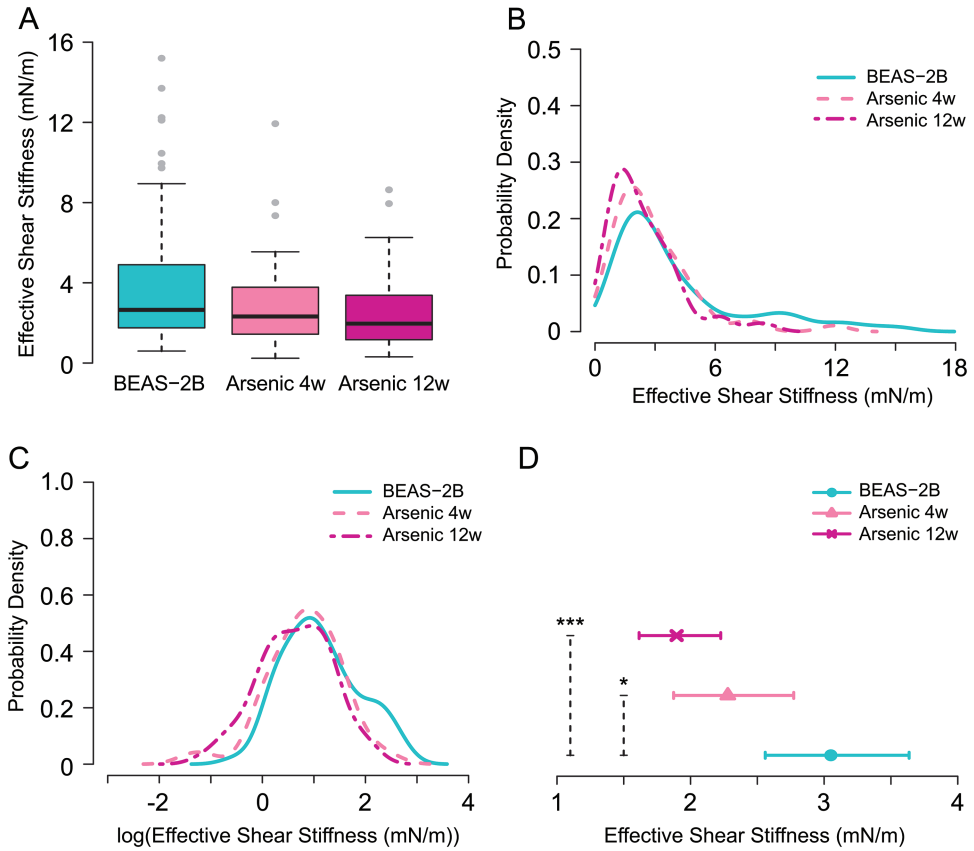

Figure 3. Plots of shear stiffness data for arsenic-exposed cell populations and the corresponding BEAS-2B control population. (**A**) Boxplots of raw data. (**B**) Estimated probability density computed from the raw data (**C**) Estimated probability density computed from log-transformed data. (**D**) Estimates of median cellular shear stiffness (mN/m) for orientation zero with 95% CIs. *P*-values are for the pairwise comparisons Arsenic 4w and BEAS-2B, and Arsenic 12w and BEAS-2B. Statistical significance of *P*-values is indicated by, $^{*}P \leq 0.05$ and $^{***}P \leq 0.001$.

Comparison of shear stiffness across treatments

Overall median shear stiffness rankings for treatment populations from low to high are the following (based on back-transformed model estimates for an orientation of zero degrees): Arsenic clones (1.84 mN/m); Arsenic 12w (1.90 mN/m); Arsenic 4w (2.28 mN/m); BEAS-2B clones (2.58 mN/m) and BEAS-2B (3.05 mN/m). Control populations (BEAS-2B and BEAS-2B clones) exhibited the highest maximum values and the widest distributions, while the Arsenic clones had the narrowest distributions. For comparison of our data to a lung cancer cell line, we measured the stiffness of A549 cells (n = 60). Empirical median and mean stiffness were 2.22 mN/m and 2.42 mN/m, respectively, with an RSD of 0.47. A549 cells exhibit stiffness that fits well within the arsenic populations, with empirical median and mean values lower than those of Arsenic 4w and higher than those of Arsenic 12w and Arsenic clones. Figure 5C presents the boxplots of raw stiffness data for the five treatment populations. In summary, our data reveal that arsenic-treated populations exhibit reduced cellular stiffness, and that passage through soft agar further decreases stiffness, resulting in the lowest stiffness values and variation for the arsenic clonal population.

Discussion

In studying the onset and progression of cellular stiffness changes during transformation, we have observed that a subtle evolution of stiffness properties is detectable. The arsenic-treated populations, Arsenic 4w and Arsenic 12w, had statistically significant reductions in cellular stiffness compared with the control population. The stiffness reduction was further magnified when Arsenic 4w cells were passaged through soft agar, which resulted in an additional reduction of stiffness in the Arsenic clones and the smallest RSD of any of the arsenic and control populations. The Arsenic clones were, therefore, delineated by the magnitude of median stiffness and also by the significantly reduced RSD, suggesting the potential value of cell stiffness for tracking the depth of transformation progression.

As discussed in the introduction, the cell culture system used to produce the various cell populations is intended to serve as a proxy for *in situ* carcinogenesis. Understanding how arsenic-induced transformation is a relevant proxy for wider cancer processes requires consideration of various topics. First, since many cancerous processes are promoted or advanced by environmental toxicants, it is important to note that the dose utilized in this experiment, which was 1 μM (130 ppb or 130 μg/L), is environmentally relevant for individuals exposed to arsenic contaminated drinking water (39,40). Contaminated water in regions such as Bangladesh has arsenic doses ranging up to 1000 ppb, placing 130 ppb well within the mid-range exposure level (39,41). Additionally, since we utilize low doses of arsenic that have low cytotoxicity, we have a prolonged exposure period during which arsenic-induced genetic and epigenetic changes can accumulate, again mirroring carcinogenesis in a wider sense (17–19). Apart from these features, recent studies indicate that arsenic may enrich stem cells and selectively transform them (42,43). Evaluation of arsenic's ability to enrich stem cells was

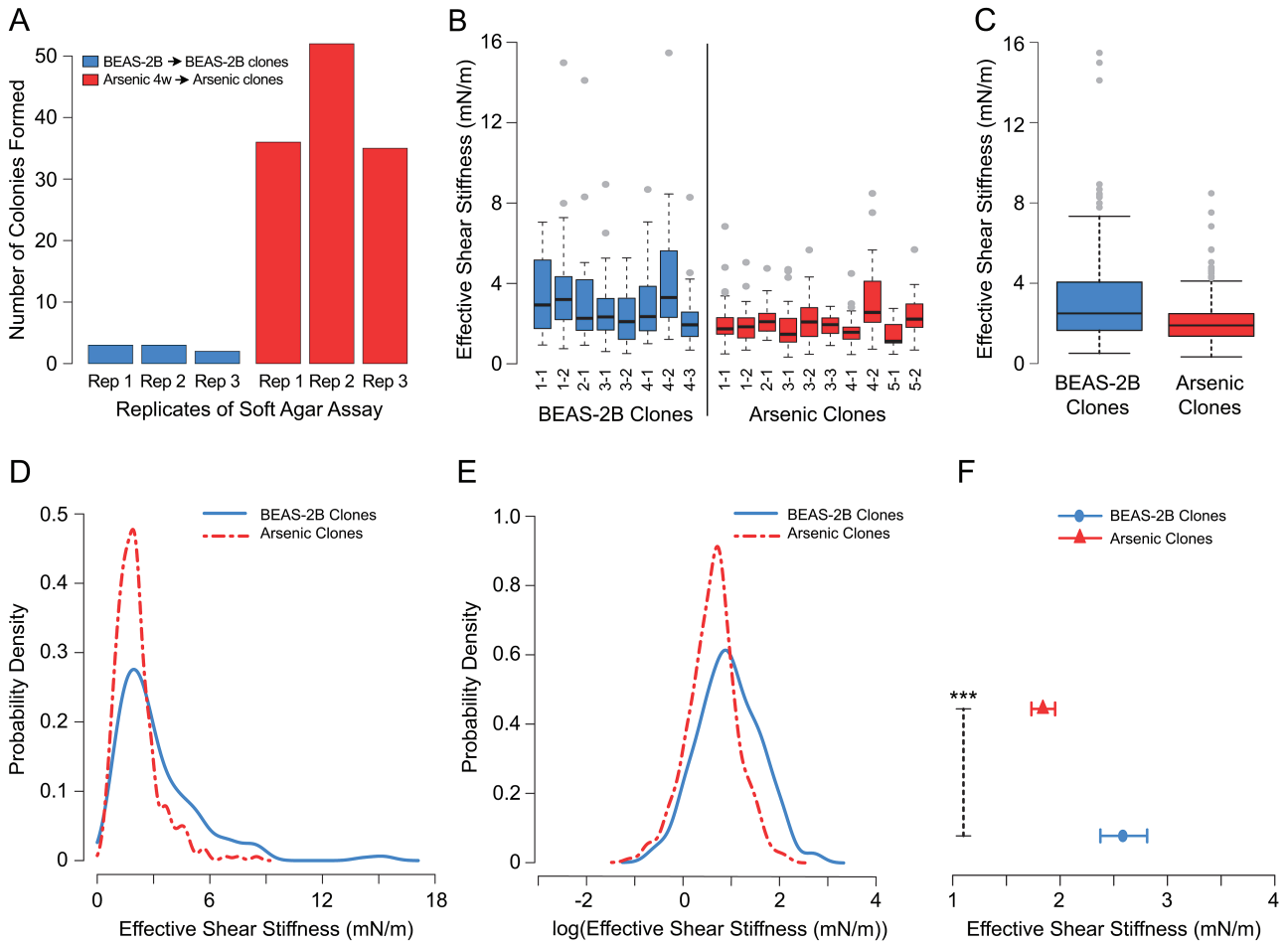

Figure 4. Plots of shear stiffness data for arsenic clonal population compared with BEAS-2B clones. (**A**) Colony count for triplicate soft agar assays of Arsenic 4w and BEAS-2B populations. BEAS-2B formed 3, 3 and 2 colonies per well, while the Arsenic 4w population formed 36, 52 and 35 colonies per well. Five Arsenic 4w clones became the arsenic clonal cell lines comprising Arsenic clones. Four BEAS-2B clones became the BEAS-2B clonal cell lines comprising the BEAS-2B clones. (**B**) Boxplots of raw data for individual clonal lines. Labels indicate treatment group, clonal line number and replicate sample number. Each replicate sample resulted in individual stiffness measurements for 14–35 cells, with sample sizes averaging 28 cells. Arsenic clones 1–5 and BEAS-2B clones 1–4 form the two treatment groups depicted in (**C**) Boxplots of raw data for pooled Arsenic clones (n = 286) and BEAS-2B clones (n = 224). (**D**) Estimated probability densities computed from the raw data. (**E**) Estimated probability densities computed from log-transformed data. (**F**) Estimates of median cellular shear stiffness (mN/m) for orientation zero with 95% CIs. Statistical significance of P-values is indicated by, ***$P \leq 0.001$.

conducted in prostate cell lines with a five times higher dose of arsenic, making it unclear to what extent this phenomenon occurs in our study since the higher dose is more cytotoxic. However, given the strong evidence, it is possible that stem cells are also selectively enriched here, and that cancer stem cells are part of the arsenic-treated populations, which would further justify their status as a viable proxy for true carcinogenic cell populations. Thus, arsenic's role in this experiment is manifold, and its capacity to promote numerous effects mirrors the wide range of deregulated processes often present during carcinogenesis.

The Arsenic clones, which received both the intracellular (arsenic) and extracellular (agar passage) modifications, exhibited the greatest decrease in cellular stiffness of any of the populations (Figure 5C). This significant reduction was accompanied by a reduced RSD and thus a narrowed distribution when Arsenic clones were compared with control clones (Figure 4). Modifications of the extracellular environment are known to mediate intracellular changes through mechanotransduction, a process that is increasingly recognized for its ability to advance carcinogenesis where changes in the tensile properties of the environment are translated to changes in mechanical integrity and pre-stress of the cell (13,44–46). Thus, we infer that the soft agar not only selected for clones exhibiting anchorage-independent growth but in doing so, advanced the process of transformation. To further contextualize the signal observed in the clones, it is instructive to compare the arsenic clonal population results with fully developed cancer cells to show that Arsenic clones are representative of later stage cancer cells. As mentioned previously, we measured A549 cells, a lung cancer cell line, and found these cancer cells to exhibit stiffness values within the range of the arsenic treated and transformed cells, corroborating that the arsenic-treated populations are in various stages of transformation. Further, the empirical RSD of the A549 cell line was the lowest of all the populations and consistent with the notion that stiffness RSD is reduced as carcinogenesis advances. The reduced stiffness and RSD observed in the Arsenic clones and A549 cells are also consistent with numerous studies that have evaluated the stiffness of cancer cells from various lineages using a variety of methods (2,47,48). For example, AFM studies conducted on cell lines have found that breast cancer MCF-7 cells had lower elastic modulus relative to benign breast

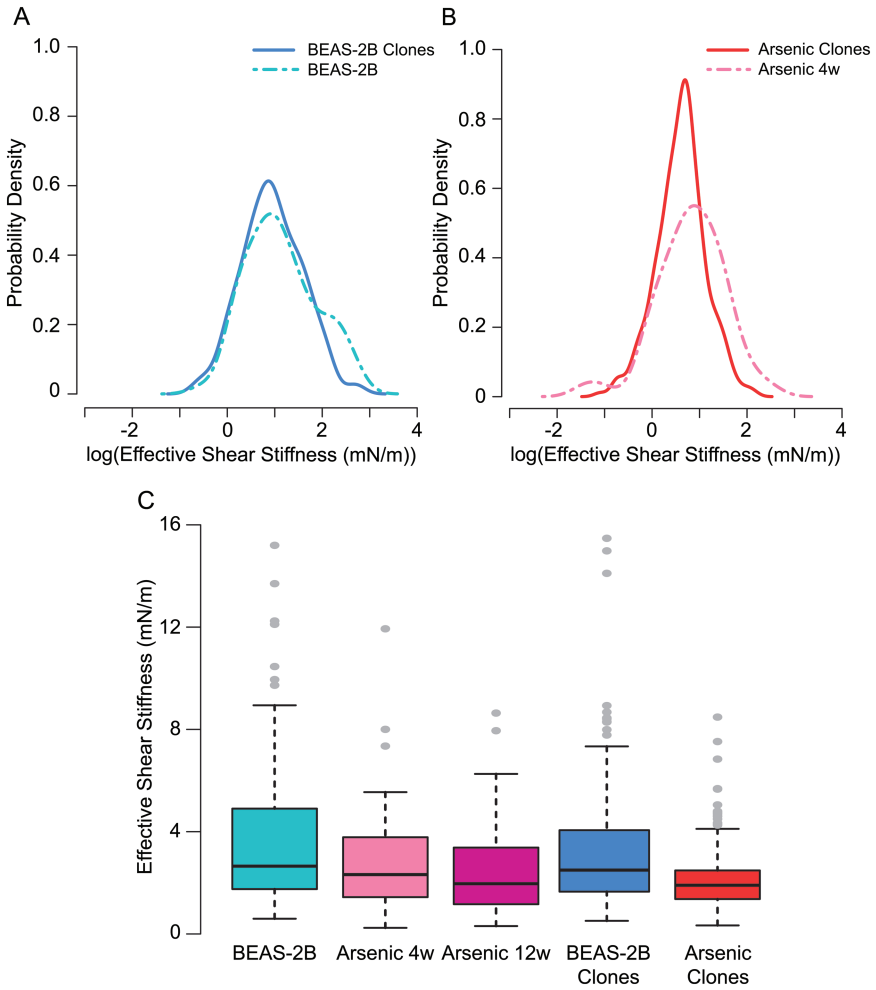

Figure 5. Graphical Summary. Estimated probability densities computed from the log-transformed measurements of cell stiffness (mN/m) to compare pre- and post-agar populations (**A**) for control BEAS-2B and BEAS-2B clones and (**B**) for Arsenic 4w and Arsenic clones. (**C**) Boxplots of raw cell stiffness data (mN/m) for all treatment groups.

MCF-10A cells (7), and that malignant prostate cancer cell lines PC-3 and LNCAp had significantly lower elastic modulus than benign prostate bpH cells (8). Studies using microfluidic optical stretchers confirm these deformability findings in numerous breast cancer cell lines, where grading of malignancy is possible based on stiffness such that metastatic cells deform more than non-metastatic cancer cells (49). Further, others have observed that there was a three-fold reduction in the standard deviation of the stiffness property in metastatic cells (2). Thus, the overall pattern confirms that the reduced stiffness and reduced RSD of the Arsenic clones seen here is consistent with the properties of established cancer cell lines and cancer cells harvested *in situ*.

In Figures 5A and B, the differences between the pre- and post-agar populations are compared. This figure illustrates the biomechanical impact of passage through agar and indicates that the passage resulted in a different distribution of responses depending on whether arsenic treatment occurred prior to agar. To statistically evaluate the impact of agar on cells, we tested whether the RSDs of cell stiffness for the pre- and post-agar populations were different and found that only the arsenic-treated population exhibited a significant reduction in RSD after agar. This observation is relevant because it provides a basis for connecting early and late stage populations through the stiffness signal and suggests that either the lowered stiffness of Arsenic 4w or intracellular changes induced by arsenic were a pre-condition for the reduced RSD. Recall, that the A549 lung cancer cells had the lowest RSD of any population, supporting the notion that RSD reflects depth of transformation. Taken together, these findings indicate that stiffness is a rich signal capable of detecting subtle shifts in cellular transformation. Further development toward a biomarker would require study of this process *in situ* and determination of the appropriate reference distribution, which may vary with respect to factors such as cell type and age.

Based on the findings of our study, which serves as a proxy for carcinogenesis *in situ*, cellular stiffness shows promise for future development as an indicator of cell transformation progression. In early stages of transformation, we observe that reduction of median stiffness values occurs after 1 month of arsenic exposure and increases as exposure progresses. Later stages of this process, represented by the Arsenic clones, exhibit additional reduction of stiffness accompanied by a reduction in the RSD of the population. Stiffness and RSD of the A549 cells support that our findings are consistent with those of a true cancer cell line. Continued development of cell stiffness as a biomarker that leverages the sensitivity of this property at the cell population level may have great value for cancer prevention, screening and diagnostic procedures.

Supplementary material

Supplementary material is available at *Carcinogenesis* online.

Funding

This work was supported by National Institute of Environmental Health Sciences (R01 ES17875, ES014454, ES005512, ES010344, P30ES000260-53); National Cancer institute (CA16087); National Science Foundation (1137475 and CBET 1604562); Danish National Research Foundation (92), National Center for Research Resources (RR029893) and Villum Fonden (17527).

Acknowledgements

We thank Hong Sun, Thomas Kluz and Brianna Loomis for their helpful laboratory assistance. Gordon Cook for figure formatting. *Conflict of Interest Statement*: None declared.

References

1. Suresh, S. (2007) Biomechanics and biophysics of cancer cells. Acta Biomater., 3, 413–438.
2. Cross, S.E. *et al.* (2008) AFM-based analysis of human metastatic cancer cells. Nanotechnology, 19, 384003.
3. Swaminathan, V. *et al.* (2011) Mechanical stiffness grades metastatic potential in patient tumor cells and in cancer cell lines. Cancer Res., 71, 5075–5080.
4. Paszek, M.J. *et al.* (2005) Tensional homeostasis and the malignant phenotype. Cancer Cell, 8, 241–254.
5. Evans, A. *et al.* (2012) Differentiating benign from malignant solid breast masses: value of shear wave elastography according to lesion stiffness combined with greyscale ultrasound according to BI-RADS classification. Br. J. Cancer, 107, 224–229.
6. Bastatas, L. *et al.* (2012) AFM nano-mechanics and calcium dynamics of prostate cancer cells with distinct metastatic potential. Biochim. Biophys. Acta, 1820, 1111–1120.
7. Li, Q.S. *et al.* (2008) AFM indentation study of breast cancer cells. Biochem. Biophys. Res. Commun., 374, 609–613.
8. Faria, E.C. *et al.* (2008) Measurement of elastic properties of prostate cancer cells using AFM. Analyst, 133, 1498–1500.
9. Lloyd, M.C. *et al.* (2016) Darwinian dynamics of intratumoral heterogeneity: not solely random mutations but also variable environmental selection forces. Cancer Res., 76, 3136–3144.
10. Tabassum, D.P. *et al.* (2015) Tumorigenesis: it takes a village. Nat. Rev. Cancer, 15, 473–483.
11. Floor, S.L. *et al.* (2012) Hallmarks of cancer: of all cancer cells, all the time? Trends Mol. Med., 18, 509–515.
12. Discher, D.E. *et al.* (2005) Tissue cells feel and respond to the stiffness of their substrate. Science, 310, 1139–1143.
13. DuFort, C.C. *et al.* (2011) Balancing forces: architectural control of mechanotransduction. Nat. Rev. Mol. Cell Biol., 12, 308–319.
14. Egeblad, M. *et al.* (2010) Dynamic interplay between the collagen scaffold and tumor evolution. Curr. Opin. Cell Biol., 22, 697–706.
15. Rahman, M.M. *et al.* (2009) Chronic exposure of arsenic via drinking water and its adverse health impacts on humans. Environ. Geochem. Health, 31, 189–200.
16. Benbrahim-Tallaa, L. *et al.* (2008) Inorganic arsenic and human prostate cancer. Environ. Health Perspect, 116, 158–164.
17. Davey, J.C. *et al.* (2007) Arsenic as an endocrine disruptor: effects of arsenic on estrogen receptor-mediated gene expression *in vivo* and in cell culture. Toxicol. Sci., 98, 75–86.
18. Flora, S.J. (2011) Arsenic-induced oxidative stress and its reversibility. Free Radic. Biol. Med., 51, 257–281.
19. Ren, X. *et al.* (2011) An emerging role for epigenetic dysregulation in arsenic toxicity and carcinogenesis. Environ. Health Perspect, 119, 11–19.
20. Andrew, A.S. *et al.* (2006) Arsenic exposure is associated with decreased DNA repair *in vitro* and in individuals exposed to drinking water arsenic. Environ. Health Perspect, 114, 1193–1198.
21. Wang, L.H. (2004) Molecular signaling regulating anchorage-independent growth of cancer cells. Mt. Sinai J. Med., 71, 361–367.
22. Fidler, I.J. *et al.* (1977) Metastasis results from preexisting variant cells within a malignant tumor. Science, 197, 893–895.
23. Eldridge, W.J. *et al.* (2016) Imaging deformation of adherent cells due to shear stress using quantitative phase imaging. Opt. Lett., 41, 352–355.
24. Passantino, L. *et al.* (2013) Sodium metavanadate exhibits carcinogenic tendencies *in vitro* in immortalized human bronchial epithelial cells. Metallomics, 5, 1357–1367.
25. Hanahan, D. *et al.* (2011) Hallmarks of cancer: the next generation. Cell, 144, 646–674.
26. Pribluda, A. *et al.* (2015) Intratumoral heterogeneity: from diversity comes resistance. Clin. Cancer Res., 21, 2916–2923.
27. Dexter, D.L. *et al.* (1978) Heterogeneity of tumor cells from a single mouse mammary tumor. Cancer Res., 38, 3174–3181.
28. Shaked, N.T. *et al.* (2010) Quantitative phase microscopy of articular chondrocyte dynamics by wide-field digital interferometry. J. Biomed. Opt., 15, 010505.
29. Shaked, N.T. *et al.* (2011) Quantitative microscopy and nanoscopy of sickle red blood cells performed by wide field digital interferometry. J. Biomed. Opt., 16, 030506.
30. Shaked, N.T. *et al.* (2010) Whole-cell-analysis of live cardiomyocytes using wide-field interferometric phase microscopy. Biomed. Opt. Express, 1, 706–719.
31. Rinehart, M. *et al.* (2012) Quantitative phase spectroscopy. Biomed. Opt. Express, 3, 958–965.
32. Bhadriraju, K. *et al.* (2002) Extracellular matrix- and cytoskeleton-dependent changes in cell shape and stiffness. Exp. Cell Res., 278, 92–100.
33. Otto, O. *et al.* (2015) Real-time deformability cytometry: on-the-fly cell mechanical phenotyping. Nat. Methods, 12, 199–202, 4 p following 202.
34. Bostock, C.J. *et al.* (1971) An evaluation of the double thymidine block for synchronizing mammalian cells at the G1-S border. Exp. Cell Res., 68, 163–168.
35. Patrício, P. *et al.* (2015) Rheology of the cytoskeleton as a fractal network. Phys. Rev. E. Stat. Nonlin. Soft Matter Phys., 92, 040702.
36. R Core Team. (2016) R: A Language and Environment for Statistical Computing. R Foundation for Statistical Computing, Vienna, Austria. https://CRAN.R-project.org
37. Pinheiro, J. *et al.* (2016) nlme: Linear and Nonlinear Mixed Effects Models. R package. https://CRAN.R-project.org/package=nlme
38. Sun, H. *et al.* (2011) Comparison of gene expression profiles in chromate transformed BEAS-2B cells. PLoS One, 6, e17982.
39. Ahsan, H. *et al.* (2006) Health Effects of Arsenic Longitudinal Study (HEALS): description of a multidisciplinary epidemiologic investigation. J. Expo. Sci. Environ. Epidemiol., 16, 191–205.
40. Colditz, G.A. *et al.* (2012) Preventability of cancer: the relative contributions of biologic and social and physical environmental determinants of cancer mortality. Annu. Rev. Public Health, 33, 137–156.
41. Chen, Y. *et al.* (2013) A prospective study of arsenic exposure, arsenic methylation capacity, and risk of cardiovascular disease in Bangladesh. Environ. Health Perspect, 121, 832–838.
42. Tokar, E.J. *et al.* (2010) Arsenic exposure transforms human epithelial stem/progenitor cells into a cancer stem-like phenotype. Environ. Health Perspect, 118, 108–115.
43. Tokar, E.J. *et al.* (2010) Arsenic-specific stem cell selection during malignant transformation. J. Natl. Cancer Inst., 102, 638–649.
44. Butcher, D.T. *et al.* (2009) A tense situation: forcing tumour progression. Nat. Rev. Cancer, 9, 108–122.
45. Ingber, D.E. (2003) Tensegrity I. Cell structure and hierarchical systems biology. J. Cell Sci., 116(Pt 7), 1157–1173.
46. Ingber, D.E. (2006) Cellular mechanotransduction: putting all the pieces together again. FASEB J., 20, 811–827.
47. Lekka, M. *et al.* (1999) Elasticity of normal and cancerous human bladder cells studied by scanning force microscopy. Eur. Biophys. J., 28, 312–316.
48. Remmerbach, T.W. *et al.* (2009) Oral cancer diagnosis by mechanical phenotyping. Cancer Res., 69, 1728–1732.
49. Guck, J. *et al.* (2005) Optical deformability as an inherent cell marker for testing malignant transformation and metastatic competence. Biophys. J., 88, 3689–3698.